

Article

Inhibition of Surface Corrosion Behavior of Zinc-Iron Alloy by Silicate Passivation

Fan Cao ^{1,†}, Peng Cao ^{1,†}, Yangyang Li ¹, Yi Wang ², Lei Shi ^{1,*} and Di Wu ^{3,*}¹ School of Materials Science and Engineering, Shandong Jianzhu University, Jinan 250101, China² Wendeng Guangrun Metal Products Co., Ltd., Weihai 266440, China; grjswy@126.com³ Shandong Provincial Eco-Environment Monitoring Center, Jinan 250014, China

* Correspondence: slcqj@sdjzu.edu.cn (L.S.); 13665312788@139.com (D.W.)

† These authors contributed equally to this paper.

Abstract: The passivation of zinc alloy coating was achieved through the utilization of both silicate and trivalent chromium passivation systems, employing a specific process formula consisting of $\text{Co}(\text{NO}_3)_2$ at a concentration of 2.5 g/L, $\text{C}_7\text{H}_5\text{O}_4$ at 3 mL/L, Na_2SiO_3 at 25 g/L, $\text{C}_6\text{H}_5\text{Na}_3\text{O}_7$ at 15 g/L, and an appropriate amount of organic accelerator. The composite passivation of silicate and tannic acid was found to be more effective than the trivalent chromium passivation film, as it successfully eliminated the dendrite structure on the coating surface and reduced surface defects. The coordination between negatively charged SiO_4^{2-} or SiO_2 micelles and Zn^{2+} results in the formation of a passivation film that exhibits lower corrosion current and higher corrosion potential compared to the trivalent chromium passivation film. Additionally, the impedance test fitting results indicate that the silicate passivation film possesses a higher resistance value. Overall, the proposed silicate passivation system presents a viable alternative to the toxic chromate passivation system, offering non-toxicity and superior protective performance relative to the trivalent chromium passivation system.

Keywords: chromate; passivation film; chromium-free passivating; corrosion



Citation: Cao, F.; Cao, P.; Li, Y.; Wang, Y.; Shi, L.; Wu, D. Inhibition of Surface Corrosion Behavior of Zinc-Iron Alloy by Silicate Passivation. *Coatings* **2023**, *13*, 1057. <https://doi.org/10.3390/coatings13061057>

Academic Editor: Alexander Modestov

Received: 12 May 2023

Revised: 28 May 2023

Accepted: 1 June 2023

Published: 7 June 2023



Copyright: © 2023 by the authors. Licensee MDPI, Basel, Switzerland. This article is an open access article distributed under the terms and conditions of the Creative Commons Attribution (CC BY) license (<https://creativecommons.org/licenses/by/4.0/>).

1. Introduction

With the development of science and technology, simple alloy coating has been unable to meet the requirements of corrosion resistance of metals, so it must be passivated [1–4]. The chromate passivation system is the passivation technology used in the surface protection industry all the time [5]. This process can not only obtain the transformation film with excellent corrosion resistance and colorful appearance but also the process is simple and the composition price is low. The passivation film formed can repair itself [6,7]. However, hexavalent chromium in chromate is highly toxic and carcinogenic, which seriously endangers human health and the natural environment. The use of hexavalent chromium in chromate is strictly restricted by the state. Although trivalent chromium is only 1% of the toxicity of hexavalent chromium, it can also be converted into hexavalent chromium during transportation and use, which also has an impact on human health [8,9]. With the enhancement of people's awareness of environmental protection and the government's strict restrictions on the use and emission of chromate, the development of chromium-free passivation technology is imperative, and good experimental results have been achieved [10,11]. At present, the chromium-free passivation process of galvanized layers used and studied at home and abroad mainly includes three categories: inorganic passivation, organic passivation, and inorganic and organic composite passivation process [12–23]. The inorganic passivation system mainly includes silicate passivation, molybdate passivation, titanium passivation, tungstate passivation, etc [24–36].

The passivation technology of silicate is one of the most promising passivation systems. Jiang et al. [37] prepared silicate-based conversion coatings by synthetic $\text{Na}_2\text{O}/\text{SiO}_2$ solutions and organic additives, dividing the zinc alloy coating into a dissolved and a

passivated part, also using atomic emission spectroscopy electrochemistry (AESEC) to find that the silicate conversion coating reduced the dissolution, which had no significant effect on the passivated component, proving that the formation of the zinc passivation film was unhindered under the actions of the silicate film. The main effect of coating on galvanized steel was to prevent the dissolution reaction of zinc. Similarly, nano-silicate coating also showed excellent protective performance in the study [38]. Sandrine et al. [39] prepared silicon base in the electrogalvanized plate in a deposition bath composed of nano-silica particles/sodium metasilicate mixture. After optimizing parameters such as the composition of sedimentation liquid, soaking time and drying temperature, Salt spray test and electrochemical impedance spectroscopy were used to evaluate its corrosion resistance. The results show that the performance of the silica-based coating is almost as good as that of the chromate coating.

At the same time, the silicate passivation system could also be combined with other inorganic passivation. Hamlaoui et al. [40] synthesized that a chromium-free passivation film based on molybdate and phosphate silicate was prepared by a simple impregnation method on the galvanized steel substrate, the corrosion behavior was compared with the typical chromate passivation film, showing that the prepared passivation film had better protection ability than the chromate passivation film.

The global commitment to environmental preservation increases due to the pollution of chromium, such that the development of chromium-free passivation process is urgently needed. Silicate passivation is very promising for the future of environmentally friendly chromium-free technology. Silicate has been extensively studied both domestically and internationally due to its numerous advantages, however, the corrosion resistance of silicate passivated film has been found to be inadequate. This paper presents a non-toxic silicate passivation formula that incorporates tannic acid to create an organic and inorganic compound passivation system. The distinctive polyphenolic structure of tannic acid confers upon it a remarkable affinity for diverse surfaces, resulting in a passivation film that is not only non-toxic but also exhibits superior corrosion resistance and densification compared to chromate passivation film. Consequently, it plays a more effective protective role for metal coatings.

2. Materials and Methods

2.1. Passivation Treatment

The chemicals utilized for the preparation of electroplating samples are of analytical grade and have been procured from various manufacturers in China. The bath must be arranged in accordance with the reagent content specified in Table 1. The cathode and anode, both made of annealed carbon steel (45 mm × 40 mm × 2 mm), are polished and cleaned prior to plating to ensure proper adhesion of the coating to the substrate. A zinc alloy coating was applied onto a Q235 thin sheet substrate (Handan Guanbiao Metal Products Manufacturing Co., Ltd., Handan, China), which was subsequently cut to dimensions of 40 mm × 45 mm × 0.8 mm. The electrodeposition process was conducted under specific conditions, including a current density of 2.0 A/dm², a temperature of 28 °C, a pH of 2, and an electrodeposition time of 15 min. It is recommended that passivation be utilized for low iron coatings, while phosphating is more suitable for high iron coatings. Therefore, the aforementioned matte zinc-iron alloy formula with low iron content is deemed appropriate for the passivation of this particular substrate. A solution for passivation was formulated utilizing Co(NO₃)₂ at a concentration of 2.5 g/L, C₇₆H₅₂O₄₆ at a concentration of 3 mL/L, Na₂SiO₃ at a concentration of 25 g/L, C₆H₅Na₃O₇ at a concentration of 15 g/L, and an appropriate quantity of organic accelerators. The composition and operational parameters of the electrodeposition bath and the configuration conditions of the passivation bath are presented in Tables 1 and 2, respectively. The electroplated sample was immersed in the prepared passivation solution for a specific duration, with continuous agitation to ensure uniform film formation. Upon completion, the sample was removed, washed, and dried.

Table 1. Composition and content of zinc alloy bath.

Component	Content
ZnO	6 g/L
NaOH	160 g/L
SEC softener	10 mL/L
SEC Complexing agent	60 g/L
FeCl ₂	3 g/L
Ethylenediamine tetraacetic acid disodium	0.8 g/L
Vanillin aldehyde	0.04 g/L

Table 2. Composition of silicate passivation solution.

Component	Content	Working Parameters
Sodium silicate	25 g/L	The pH was 1 to 2, the temperature was 25 °C and the time was 30 s.
Cobalt nitrate	2.5 g/L	
Sodium citrate	15 g/L	
Tannins	2–4 g/L	
Organic promoter	Right amount	

The prescribed sequence entails the following steps: polishing, water immersion, oil elimination, water immersion, rust elimination, water immersion, activation, water immersion, electrodeposition, and water immersion. The constituents and proportions of the zinc alloy bath are delineated in Table 1.

Three samples prepared under the same conditions were labeled as No. 1, 2 and 3, respectively. No. 1 is not subjected to any treatment, No. 2 is passivated with an ordinary trivalent chromium system, and No. 3 is passivated with a self-configured silicate passivating solution. The specific composition, content and process are shown in Table 2.

2.2. Microstructure Characterization

Bruker D8 Advance X-ray diffractometer (XRD) (Bruker, Saarbrücken, Germany) was used to detect the sample for phase composition. The radiation source was Cu K α filtered by Ni, the wavelength was 1.5059 Å, the scanning interval was $10^\circ \leq 2\theta \leq 90^\circ$, and the scanning speed was $2^\circ/\text{min}$. The sample test results were analyzed with Jade software. ZEISS SUPRA™ 55 scanning electron microscope (SEM) (ZEISS, Oberkochen, Germany) was used to observe the morphology of the samples. The acceleration voltage was 20–25 kV and the vertical spot diameter was 2–3 μm . The surface topography was measured by KathMatic KX-X1000 laser confocal microscope (KathMatic, Nanjing, China).

2.3. Evaluation of Corrosion Performance

The corrosion resistance of the samples was characterized by neutral salt spray measurements and an electrochemical measurement. The ASR-60 salt spray testing machine was used to simulate the corrosion environment, and the corrosion resistance of the samples was characterized by recording the time from the beginning of sample placement until the sample produced white rust.

Electrochemical measurements were performed in a conventional three-electrode cell using a platinum wire as the counter electrode, a saturated calomel electrode as the reference, and a sample with an exposed area of 1 cm² as the working electrode. Shanghai Chenhua CH760E electrochemical workstation was used. The open circuit potential was monitored for 10 min. Next, electrochemical impedance spectroscopy (EIS) measurements were performed in 3.5% NaCl solution with an amplitude of 5 mV at a frequency range of 10 kHz to 1 Hz. After EIS, the potentiodynamic polarization test (Tafel) was performed at a

scanning speed of 1 mV/s. The corrosion current density tests can be used to calculate the corrosion velocity of the matrix metal by the following equation:

$$V = \frac{A}{nF} \cdot I_{\text{corr}} \quad (1)$$

In the formula, V represents the corrosion velocity of the cladding layer, and the higher the value, the worse the corrosion resistance. A is the number of metal atoms, F is a constant, and n is the atomic valence. It can be seen from the above equation that the corrosion velocity V of passivation coating is linearly related to the corrosion current density I_{corr} . The fast corrosion speed was produced with the high I_{corr} value, reducing the corrosion resistance of the metal. In addition, it should be understood that the testing sequence of Tafel and EIS should not be reversed, because the Tafel test will affect the surface state of the passivation film, resulting in inaccurate EIS test results. The test should be conducted several times to ensure the reproducibility of the experimental results.

3. Results and Discussion

3.1. Surface Morphology and Composition Analysis

The X-ray diffraction (XRD) pattern depicted in Figure 1 illustrates the crystal structure of the non-passivation coating and the coating treated with various passivation modes. Analysis of the figure reveals that no new peak generation or displacement is observed in the XRD pattern between the coating and the passivation-treated coating. This observation suggests that the passivation film applied to the coating does not influence the crystal structure during the XRD measurement process. There is speculation that the passivation film may be insufficiently thick, and the constituents thereof are not readily discernible. The results of Zhang et al. [41] showed that XRD showed no significant difference between electroplating and sodium molybdate conversion coating, indicating that the passivation film thickness was very thin, which was consistent with the experimental results. Presumably, the trivalent chromium and silicate passivation films are very small, typically between 5–15 nm, and almost impossible to see.

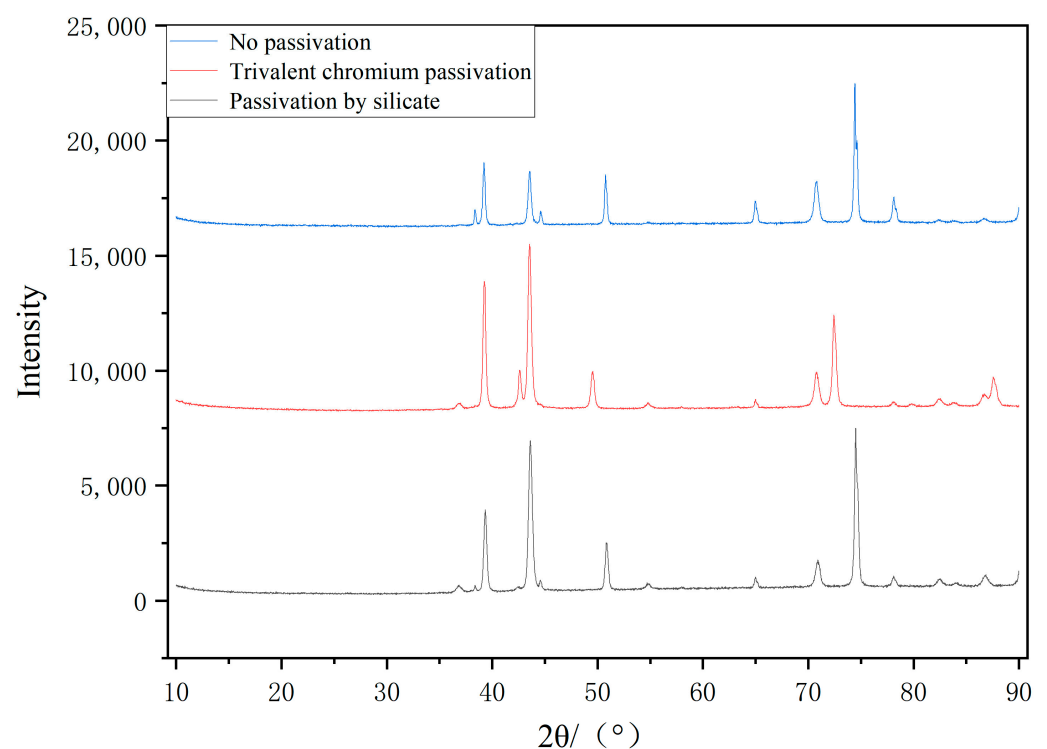


Figure 1. X-ray diffraction pattern of non-passivated coating and the passivated coating.

Figure 2a,b depict the microscopic magnification of the unpassivated sample at $3k\times$ and $5k\times$, respectively. The images reveal a rough surface with significant particle adhesion and numerous dendrite-shaped structures present in the area. The increase in structural defects results in a larger surface area and a decline in corrosion resistance performance. The formation of defects during the coating preparation process is the underlying cause. The occurrence of these defects can be attributed to the fluctuation in current density and the non-uniform distribution of ions within the plating solution during the coating preparation process. Figure 2c,d depict the microscopic magnification of the trivalent chromium passivated sample at $3k\times$ and $5k\times$, respectively. The figures demonstrate that the surface morphology after trivalent chromium treatment is relatively flat, with the disappearance of the dendritic structure and the absence of large particles. However, small tissue particles are still present. Sandberg et al. [42] demonstrated that the surface composition of the sample may consist of a complex mixture of $\text{Cr}_2(\text{SO}_4)_3$, Cr_2O_3 , $\text{Cr}(\text{OH})_3$, ZnSO_4 , and ZnO compounds. Figure 2d reveals the presence of surface defects, including holes and flaky films, which suggest non-uniform formation of passivation films [43]. This suggests that the majority of surface defects in the coating can be remedied, leading to an enhancement in corrosion resistance. However, a small number of surface defects remain unresolved. Figure 2e,f depict the microscopic magnification of the silicate passivated sample at $3k\times$ and $5k\times$, respectively. The images reveal a flat surface devoid of any discernible defects, complete absence of dendritic structure, and uniformity in the tissue particles. These figures suggest that the coordination of negatively charged SiO_2^- or SiO_2 gel with Zn^{2+} may lead to the formation of the passivation film. The incorporation of tannic acid facilitates the generation of hydroxyl and carboxyl groups essential for the passivation of the film and enhances its formation. Upon comparison of the surface morphology resulting from three distinct treatment methods, it is evident that the unpassivated coating exhibits a greater prevalence of large metal particles and dendrite structures. While chromate passivation serves to essentially eliminate surface defects, small tissue particles remain present. In contrast, silicate passivation treatment results in the complete eradication of surface defects, yielding a uniform and compact surface.

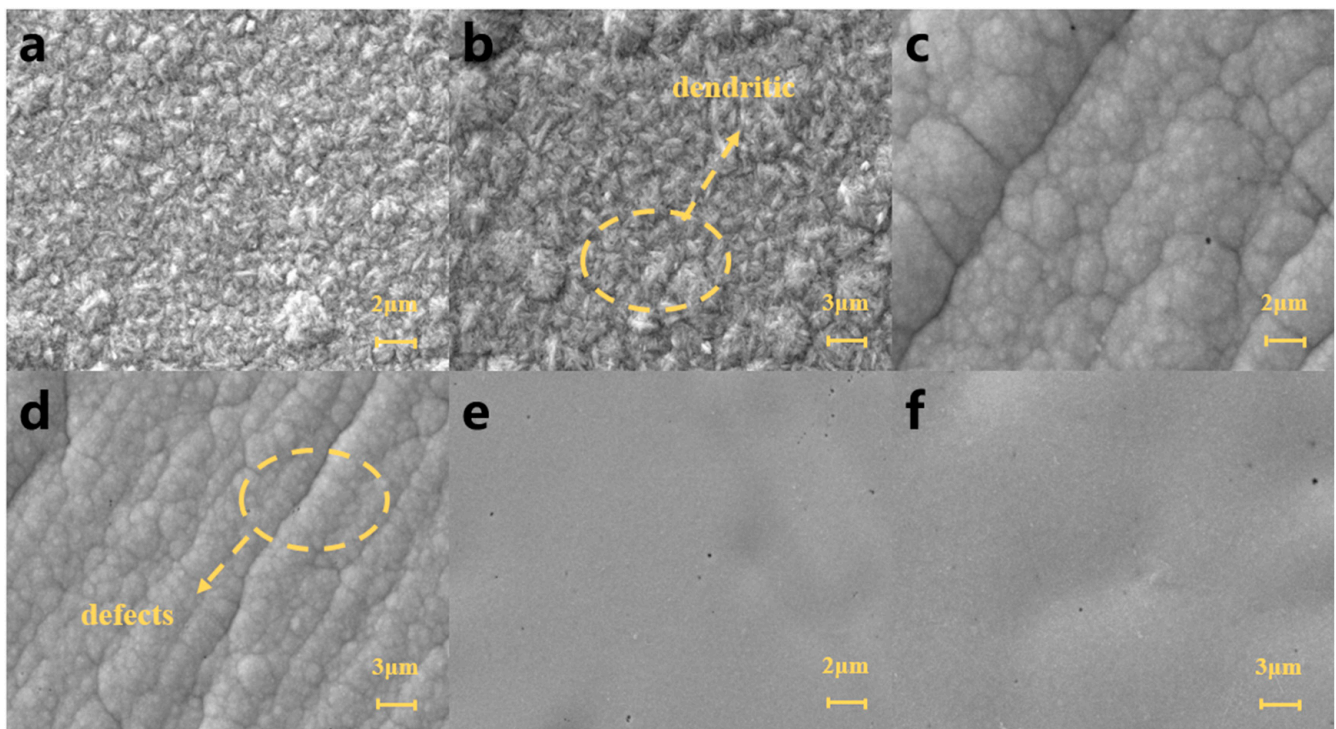


Figure 2. Unpassivated SEM ((a): $3k\times$, (b): $5k\times$), trivalent chromium passivated SEM ((c): $3k\times$, (d): $5k\times$), silicate passivated SEM ((e): $3k\times$, (f): $5k\times$).

3.2. Corrosion Resistance of Passivation Film

3.2.1. Polarization Curve

Figure 3 showed the Tafel curves of the three samples in 3.5%NaCl solution. From the figure, it was easily observed that the corrosion rate in the NaCl medium was controlled by the cathode. Table 3 summarized the corrosion current (I_{corr}), corrosion potential (E_{corr}) and corresponding polarization resistance (R_p) of the samples. As shown in the table, the I_{corr} value of the trivalent chromium passivated sample was $1.422 \times 10^{-2} \mu\text{A}\cdot\text{cm}^{-2}$, and the I_{corr} value of the silicate passivated sample was $0.853 \times 10^{-2} \mu\text{A}\cdot\text{cm}^{-2}$, which were lower than the I_{corr} value of unpassivated sample (the I_{corr} value was $5.597 \times 10^{-2} \mu\text{A}\cdot\text{cm}^{-2}$). The corrosion current density was inversely proportional to the corrosion resistance of the film. The smaller the current density, the better the corrosion resistance. The data indicates that the unpassivated zinc alloy layer exhibited the highest current density, which decreased significantly upon passivation. Conversely, the silicate passivated workpiece demonstrated the lowest current density and the highest corrosion resistance. These findings suggest that silicate passivation may serve as a viable alternative to trivalent chromium passivation systems for coating protection.

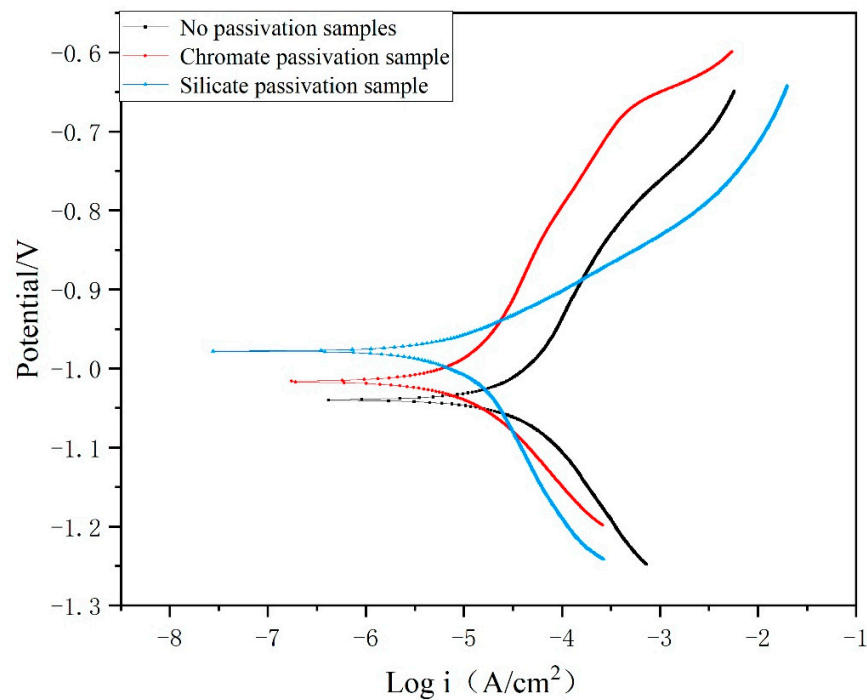


Figure 3. Dynamic potential polarization curves of samples with different surface treatment processes in 3.5% NaCl solution.

Table 3. Corrosion potential (E_{corr}), Corrosion current (I_{corr}) and polarization resistance (R_p) of samples with different surface treatment processes.

The Surface Type	E_{corr} (mV vs. SCE)	I_{corr} ($10^{-2} \mu\text{A cm}^{-2}$)	R_p (Ωcm^{-2})
No passivation	−1040	5.597	739
Trivalent chromium passivation	−1017	1.422	2549
Passivation of silicate	−978	0.853	2679

As could be seen in Table 3, the corrosion potential of the unpassivated sample with an E_{corr} value of -1.040 V. After passivation was the lowest, the corrosion potential of the sample increased significantly. The E_{corr} value of trivalent chromium passivation was -1.017 V, and that of silicate passivation with a positive potential shift was -0.978 V,

indicating that the corrosion resistance of the film was significantly improved. Silicate passivation film had the best corrosion resistance.

3.2.2. Impedance Study

Figure 4 displays the EIS curve of three samples immersed in a 3.5% NaCl solution. The radius of the impedance arc is a reliable indicator of the strength of corrosion resistance. The electrochemical parameter that exhibits the highest reliability in characterizing the corrosion resistance of the samples is the impedance value at low frequency and the enhanced high-frequency region, as determined through electrochemical impedance measurement. It was obvious from the figure that the samples without passivation have the smallest arc radius and impedance, and the worst corrosion resistance. After passivation surface covered with a layer of passivation film, The radius of low-frequency capacitive reactance arc increased significantly, the high-frequency area was also improved, the corrosion impedance values were increased, showing that the passivation membrane could obviously increase the corrosion resistance of the substrate, and the main body in physical isolation corrosive medium and chemical inhibition of charge transfer and electrochemical corrosion. There might also be a conversion film on the unpassivated sample, which might be a natural oxide film formed under natural conditions and could not provide the same performance as the passivated film. The corrosion resistance of silicate passivation film was the best in the passivation film formed.

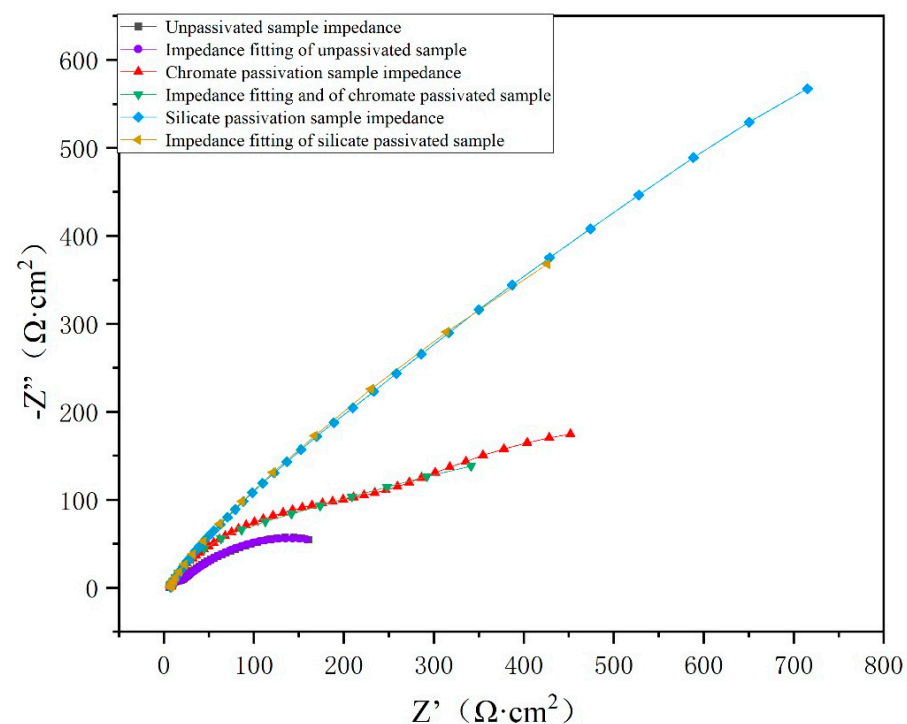


Figure 4. EIS curves of samples with different surface treatment processes in 3.5% NaCl solution.

The equivalent circuit diagram employed in fitting is depicted in Figure 5, wherein R_s denotes the solution resistance, R_a represents the coating resistance, R_{ct} signifies the charge transfer resistance, and CPE-1 and CPE-2 denote two constant phase elements. Figure 6 reveals the presence of minute cracks on the passivation film, which fragment it into multiple sections. The parallel resistances of these sections cannot be disregarded, thereby rendering CPE-1 non-equivalent to capacitance C . Additionally, the passivation film's cracks allow ions in NaCl solution to traverse it and access the substrate, making CPE-2 non-equivalent to capacitance C . Table 4 displays the fitting outcomes of the EIS data for the three samples. The R_p value, which is the sum of R_s , R_a , and R_{ct} , was observed to be $3010.84 \Omega \cdot \text{cm}^2$ for the silicate passivated sample, $1075.10 \Omega \cdot \text{cm}^2$ for the trivalent

chromium passivated sample, and $265.78 \Omega \cdot \text{cm}^2$ for the non-passivated sample, as indicated in the table. The significantly lower R_p value of the non-passivated sample suggests that passivation can greatly enhance the coating’s corrosion resistance. Furthermore, the highest R_p value was observed for the silicate passivated film, indicating its superior protective ability.

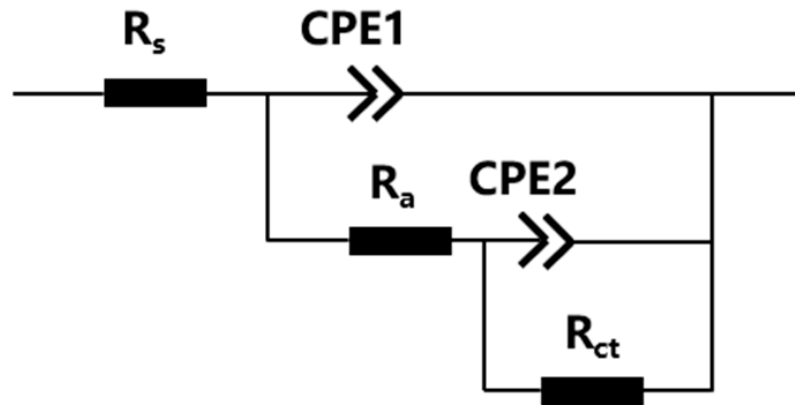


Figure 5. Quasi and equivalent circuit model.

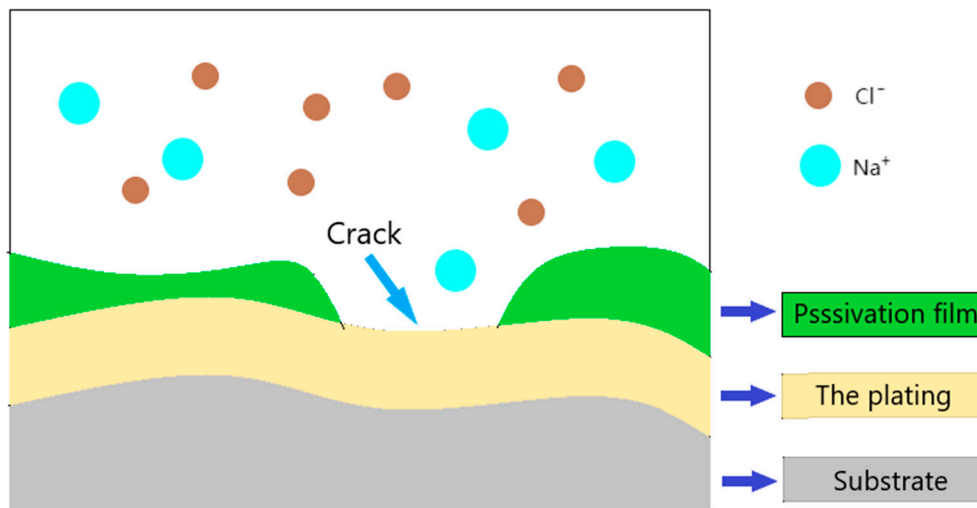


Figure 6. Samples surface microcosmic diagram.

Table 4. EIS fitting parameters of samples with different surface treatments.

The Surface Type	$R_s/\Omega \cdot \text{cm}^2$	CPE1- $T(10^{-4}/\Omega^{-1} \cdot \text{cm}^{-2} \cdot \text{s}^n)$	$R_{ct}/\Omega \cdot \text{cm}^2$	$R_a/\Omega \cdot \text{cm}^2$	CPE2- $T(10^{-4}/\Omega^{-1} \cdot \text{cm}^{-2} \cdot \text{s}^n)$	$R_p/\Omega \cdot \text{cm}^2$
No passivation	6.20	341.31	249.10	10.48	11.88	265.78
Trivalent chromium passivation	7.20	27.31	958.80	109.10	1.52	1075.10
Passivation of silicate	7.04	1.00	2795.00	208.80	2.94	3010.84

3.2.3. Salt Spray Test to Analyse Corrosion Resistance

Three distinct surface treatment processes were subjected to a salt spray test in a controlled environment to replicate hot and humid conditions. Following a 72-h exposure, the samples were retrieved and analyzed. The outcomes of the experiment are presented in Figure 7. The silicate passivation sample exhibited a minor presence of white rust on its surface, while the trivalent chromium passivation sample displayed a significant amount of white rust, indicating the presence of red rust in the passivation sample. In the context of a humid and hot salt spray environment, the chloride ions present in the brine adhere to the

surface of the passivation film and infiltrate the zinc coating, resulting in an electrochemical reaction. This reaction involves the oxidation and reduction of Cl^- and Zn, leading to the formation of ZnCl_2 , commonly referred to as white rust, which ultimately deteriorates the passivation film. The duration of white rust formation is contingent upon the surface characteristics of the passivation film. The formation of white rust was impeded by both the dense passivation film and the thick film. The passivation film's surface exhibited pitting corrosion in areas with defects, leading to the onset of white rust. Destruction of the zinc coating and subsequent Cl^- infiltration into the iron substrate's surface resulted in corrosion of the metal substrate and the occurrence of red rust. The sample treated with silicate passivation exhibited the lowest occurrence of white rust, indicating superior corrosion resistance of the passivation film, followed by the trivalent chromium passivation film. Conversely, the unpassivated sample displayed red embroidery and corrosion of the surface metal matrix. These observations suggest that passivation reduces surface defects and minimizes corrosion sites, thereby prolonging the lifespan of the metal matrix, a finding that aligns with previous SEM analyses.

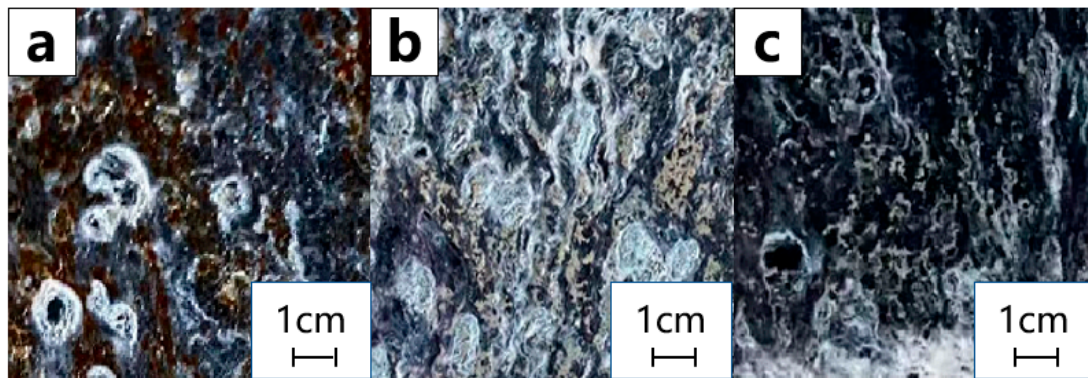


Figure 7. Surface of three samples after 72 h salt spray measures ((a): unpassivated sample, (b): trivalent chromium passivated sample, (c): silicate passivated sample).

In conclusion, the experimentation of three distinct surface treatments on samples has revealed a significant presence of dendrite structures and sizable particles on the surface of the coating that has not undergone passivation treatment. The existence of these imperfections is likely to instigate corrosion, thereby impeding the metal matrix from achieving its intended service life and leading to premature failure. Both chromate and silicate passivation techniques have the ability to eliminate surface defects; however, the treatment efficacy of silicate passivation surpasses that of chromate passivation. This conclusion is supported by the SEM images, electrochemical test results, and salt spray test of the two samples. Furthermore, the silicate passivation process can effectively eliminate chromium ion pollution while ensuring adequate protection.

4. Conclusions

By characterizing the layers of different surface treatment processes, the following conclusions are drawn:

The passivation film had no effect on the crystal structure of the coating, and the thickness was very thin. However, by observing the microstructure of SEM, it could be seen that the dendrites structure of the coating surface would be changed by the passivation layer, so as to reduce the surface defects and the specific surface area. Compared with the micro-topography after the two passivation processes, the passivation film formed by the silicate system provided in this paper has better protection ability.

Silicate passivation film might be formed by the coordination of negatively charged SiO_2^{2-} or SiO_2 micelle and Zn^{2+} . The addition of tannic acid provides the hydroxyl and carboxyl groups needed for the passivation film to promote the formation of the film.

Through the light performance characterization methods such as morphology analysis, electrochemical measurements, compared the silicate passivation system proposed in this paper and the trivalent chromium passivation system, and it has been proved that using this formula form of passivation film than traditional trivalent chromium passivation film corrosion resistant performance was better, which could replace the toxic trivalent chromium passivation system effectively.

The traditional research on chromium-free passivation solutions has neglected to prioritize the examination of reagent content and formula technology, while disregarded the pivotal role of the reaction mechanism. A comprehensive understanding of the experimental principles underlying the reaction is essential for guiding future research endeavors. This study examines the passivation liquid of silicate tannic acid complex, which is currently in the laboratory research phase. To achieve industrial application, extensive application data must be gathered and the passivation process must be continuously optimized. Additionally, the passivation reaction mechanism warrants further investigation.

Author Contributions: Conceptualization, F.C. and L.S.; methodology, F.C.; software, P.C.; validation, F.C., P.C. and Y.L.; formal analysis, F.C. and P.C.; investigation, F.C., P.C. and Y.L.; resources, L.S.; data curation, F.C., P.C. and Y.W.; writing—original draft preparation, F.C. and P.C.; writing—review and editing, F.C., P.C. and L.S.; supervision, L.S.; project administration, F.C., L.S. and D.W.; funding acquisition, F.C., L.S. and D.W. All authors have read and agreed to the published version of the manuscript.

Funding: This work was financially supported by the Shandong Provincial Natural Science Foundation, China (No. ZR202108100033); Shandong Province Science and Technology Small and Medium Enterprises Innovation Ability Improvement Project, China (No. 2022TSGC2561); Youth Special Project of Qingdao Applied Basic Research Program (No. 18-2-2-70-jch).

Institutional Review Board Statement: Not applicable.

Informed Consent Statement: Not applicable.

Data Availability Statement: The data presented in this study are available in this article.

Acknowledgments: The authors want to thank Jinan Institute of Quantum Technology for the assistance with the XRD and SEM measurements.

Conflicts of Interest: The authors declare no conflict of interest.

References

1. Kong, G.; Lu, J.; Zhang, S.; Che, C.; Wu, H. A comparative study of molybdate/silane composite films on galvanized steel with different treatment processes. *Surf. Coat. Technol.* **2010**, *205*, 545–550. [[CrossRef](#)]
2. Long, H.; Chen, L.; Dong, B.; Sun, Y.; Yan, Y.; Chen, C. The electronic properties and surface chemistry of passive film on reinforcement: Effect of composition of simulated concrete pore solution. *Constr. Build. Mater.* **2022**, *360*, 129567. [[CrossRef](#)]
3. Zhang, G.; Jiang, E.; Wu, L.; Tang, A.; Atrens, A.; Pan, F. Active corrosion protection of phosphate loaded PEO/LDHs composite coatings: SIET study. *J. Magnes. Alloys* **2022**, *10*, 1351–1357. [[CrossRef](#)]
4. Chen, Z.; Liu, X.; Kan, X.; Wang, Z.; Zhu, R.; Yang, W.; Wu, Q.; Shezad, M. Phosphate coatings evolution study and effects of ultrasonic on soft magnetic properties of FeSiAl by aqueous phosphoric acid solution passivation. *J. Alloys Compd.* **2019**, *783*, 434–440. [[CrossRef](#)]
5. Sheu, H.H.; Lee, H.B.; Jian, S.Y.; Hsu, C.Y.; Lee, C.Y. Investigation on the corrosion resistance of trivalent chromium conversion passivate on electroplated Zn–Ni alloy. *Surf. Coat. Technol.* **2016**, *305*, 241–248. [[CrossRef](#)]
6. Yuan, M.; Lu, J.; Kong, G.; Che, C. Self healing ability of silicate conversion coatings on hot dip galvanized steels. *Surf. Coat. Technol.* **2011**, *205*, 4507–4513. [[CrossRef](#)]
7. Thakur, A.; Kaya, S.; Kumar, A. Recent innovations in nano container-based self-healing coatings in construction industry. *Curr. Nanosci.* **2022**, *18*, 203–216. [[CrossRef](#)]
8. Monga, A.; Fulke, A.B.; Dasgupta, D. Recent developments in essentiality of trivalent chromium and toxicity of hexavalent chromium: Implications on human health and remediation strategies. *J. Hazard. Mater. Adv.* **2022**, *7*, 100113. [[CrossRef](#)]
9. Huang, C.; Chen, Y.; Lin, C. High-temperature oxidation resistance of hot stamping steel with chromium coating electroplated in trivalent chromium bath. *Mater. Today Commun.* **2022**, *33*, 104663. [[CrossRef](#)]
10. Winn, D.; Dalton, W. Chromium-free corrosion solutions: Silica-based electrolytic method offers viable alternative to both hex- and trivalent-chromate passivates. *Met. Finish.* **2008**, *106*, 70–74. [[CrossRef](#)]

11. Yang, T.; Chen, W.; Li, X.; Song, J.; Dong, L.; Fu, Y. Environment-friendly and chromium-free passivation of copper and its alloys. *Mater. Today Commun.* **2021**, *29*, 102826. [[CrossRef](#)]
12. Liu, Q.; Zhang, X.; Zhou, W.; Ma, R.; Du, A.; Fan, Y.; Zhao, X.; Cao, X. Improved anti-corrosion behaviour of an inorganic passive film on hot-dip galvanised steel by modified graphene oxide incorporation. *Corros. Sci.* **2020**, *174*, 108846. [[CrossRef](#)]
13. Safaruddin, A.; Bermundo, J.; Jallorina, M.; Yamamoto, A.; Uraoka, Y. Spray pyrolyzed fluorinated inorganic-organic passivation for solution-processed a-InZnO thin-film transistors. *Mater. Sci. Semicond. Process.* **2022**, *146*, 106669. [[CrossRef](#)]
14. Qi, W.; Zhou, X.; Li, J.; Cheng, J.; Li, Y.; Ko, M.; Zhao, Y.; Zhang, X. Inorganic material passivation of defects toward efficient perovskite solar cells. *Sci. Bull.* **2020**, *65*, 2022–2032. [[CrossRef](#)] [[PubMed](#)]
15. Banczek, E.P.; Terada, M.; Rodrigues, P.R.P.; Costa, I. Study of an alternative phosphate sealer for replacement of hexavalent chromium. *Surf. Coat. Technol.* **2010**, *205*, 2503–2510. [[CrossRef](#)]
16. Guo, S.; Xu, D.; Jiang, G.; Guo, Y.; Jing, Z. Sulfate corrosion and phosphate passivation of Ni-based alloy in supercritical water. *J. Supercrit. Fluids* **2022**, *184*, 105564. [[CrossRef](#)]
17. Liu, Q.; Ma, R.; Du, A.; Zhang, X.; Fan, Y.; Zhao, X.; Zhang, S.; Cao, X. Investigation on structure and corrosion resistance of complex inorganic passive film based on graphene oxide. *Corros. Sci.* **2019**, *150*, 64–75. [[CrossRef](#)]
18. Lei, S.; Wang, S.; Zhong, H.; Ma, X.; Cao, Z. Performance and corrosion resistance mechanism of SA-Al composite hydrophobic coating on electrolytic manganese surface. *Surf. Coat. Technol.* **2021**, *419*, 127290. [[CrossRef](#)]
19. Li, J.; Sun, C.; Roostaei, M.; Mahmouidi, M.; Fattahpour, V.; Zeng, H.; Luo, J. Characterization and corrosion behavior of electroless Ni-Mo-P/Ni-P composite coating in CO₂/H₂S/Cl⁻ brine: Effects of Mo addition and heat treatment. *Surf. Coat. Technol.* **2020**, *403*, 126416. [[CrossRef](#)]
20. Firouzi-Nerbin, H.; Nasirpour, F.; Moslehifard, E. Pulse electrodeposition and corrosion properties of nanocrystalline nickel-chromium alloy coatings on copper substrate. *J. Alloys Compd.* **2020**, *822*, 153712. [[CrossRef](#)]
21. Foster, K.; Claypool, J.; Fahrenholtz, W.G.; O'Keefe, M.; Nahlawi, T.; Almodovar, F. Characterization of cobalt containing and cobalt-free trivalent chromium passivations on γ -ZnNi coated steel substrates. *Thin Solid Films* **2021**, *735*, 138894. [[CrossRef](#)]
22. Karthikeyan, P.; Malathy, M.; Rajavel, R. Poly(o-phenylenediaminecoaniline)/ZnO coated on passivated low nickel stainless steel. *J. Sci. Adv. Mater. Devices* **2017**, *2*, 86–92. [[CrossRef](#)]
23. Silva, J.; Torresi, S.; Torresi, R. Polyaniline/poly (methylmethacrylate) blends for corrosion protection: The effect of passivating dopants on different metals. *Prog. Org. Coat.* **2007**, *58*, 33–39. [[CrossRef](#)]
24. Qin, B.; Ma, L.; Wang, S.; Hou, C.; Zhou, S. Construction of a sandwich-like Gr/Ni composite coating on AZ91D magnesium alloy to achieve excellent corrosion and wear resistances in the seawater. *Diam. Relat. Mater.* **2022**, *130*, 109400. [[CrossRef](#)]
25. Xu, R.; He, T.; Yang, R.; Da, Y.; Chen, C. Application zinc silicate-potassium silicate coating for anticorrosion of steel bar in autoclaved aerated concrete. *Constr. Build. Mater.* **2020**, *237*, 117521. [[CrossRef](#)]
26. Cai, Q.; Wang, L.; Wei, B.; Liu, Q. Electrochemical performance of microarc oxidation films formed on AZ91D magnesium alloy in silicate and phosphate electrolytes. *Surf. Coat. Technol.* **2006**, *200*, 3727–3733. [[CrossRef](#)]
27. Oliveira, L.; Correa, O.; Santos, D.; Páez, A.; Oliveira, M.; Antunes, R. Effect of silicate-based films on the corrosion behavior of the API 5L X80 pipeline steel. *Corros. Sci.* **2018**, *139*, 21–34. [[CrossRef](#)]
28. Yuan, M.; Lu, J.; Kong, G. Effect of SiO₂:Na₂O molar ratio of sodium silicate on the corrosion resistance of silicate conversion coatings. *Surf. Coat. Technol.* **2010**, *204*, 1229–1235. [[CrossRef](#)]
29. Wu, T.; Blawert, C.; Serdechnova, M.; Karlova, P.; Dovzhenko, G.; Wieland, D.C.F.; Stojadinovic, S.; Vasilic, R.; Wang, L.; Wang, C.; et al. Role of phosphate, silicate and aluminate in the electrolytes on PEO coating formation and properties of coated Ti₆Al₄V alloy. *Appl. Surf. Sci.* **2022**, *595*, 153523. [[CrossRef](#)]
30. Wang, Q.; Cheng, X.; Zheng, L.; Ye, P.; Li, M.; Shen, L.; Li, J.; Zhang, D.; Gu, Z.; Yu, Y. Enhanced interfacial and electrical characteristics of 4H-SiC MOS capacitor with lanthanum silicate passivation interlayer. *Appl. Surf. Sci.* **2017**, *410*, 326–331. [[CrossRef](#)]
31. Tristijanto, H.; Ilman, M.; Iswanto, P. Corrosion Inhibition of Welded of X—52 Steel Pipelines by Sodium Molybdate in 3.5% NaCl Solution. *Egypt. J. Pet.* **2020**, *29*, 155–162. [[CrossRef](#)]
32. Osipenko, M.; Kharytonau, D.; Kasach, A.; Ryl, J.; Adamiec, J.; Kurilo, I. Inhibitive effect of sodium molybdate on corrosion of AZ31 magnesium alloy in chloride solutions. *Electrochim. Acta* **2022**, *414*, 140175. [[CrossRef](#)]
33. Alves, A.; Wenger, F.; Ponthiaux, P.; Celis, J.; Pinto, A.; Rocha, L.; Fernandes, J. Corrosion mechanisms in titanium oxide-based films produced by anodic treatment. *Electrochim. Acta* **2017**, *234*, 16–27. [[CrossRef](#)]
34. Micallef, C.; Chiu, C.; Zhuk, Y.; Aria, A. Rapid surface finishing of chemical vapour deposited tungsten carbide hard coatings by electropolishing. *Surf. Coat. Technol.* **2021**, *428*, 127900. [[CrossRef](#)]
35. Tsai, C.; Liu, J.; Chen, P.; Lin, C. A roll coating tungstate passivation treatment for hot-dip galvanized sheet steel. *Surf. Coat. Technol.* **2011**, *205*, 5124–5129. [[CrossRef](#)]
36. Qin, W.; Xi, X.; Zhang, L.; Wang, M.; Nie, Z. Effect of cathodic current density on the microstructure and performance of W-ZrO₂ composites coating prepared in Na₂WO₄-WO₃-ZrO₂ molten salt. *Surf. Coat. Technol.* **2022**, *440*, 128497. [[CrossRef](#)]
37. Jiang, L.; Wolpers, M.; Volovitch, P.; Ogle, K. An atomic emission spectroelectrochemical study of passive film formation and dissolution on galvanized steel treated with silicate conversion coatings. *Surf. Coat. Technol.* **2012**, *206*, 3151–3157. [[CrossRef](#)]
38. Thakur, A.; Kaya, S.; Kumar, A. Recent Trends in the Characterization and Application Progress of Nano-Modified Coatings in Corrosion Mitigation of Metals and Alloys. *Appl. Sci.* **2023**, *13*, 730. [[CrossRef](#)]

39. Dalbin, S.; Maurin, G.; Nogueira, R.; Persello, J.; Pommier, N. Silica-based coating for corrosion protection of electrogalvanized steel. *Surf. Coat. Technol.* **2005**, *194*, 363–371. [[CrossRef](#)]
40. Hamlaoui, Y.; Tifouti, L.; Pedraza, F. Corrosion behaviour of molybdate–phosphate–silicate coatings on galvanized steel. *Corros. Sci.* **2009**, *51*, 2455–2462. [[CrossRef](#)]
41. Zhang, M.; Mu, S.; Guan, Q.; Li, W.; Du, J. A high anticorrosive chromium-free conversion coating prepared with an alkaline conversion bath on electroless Ni–P coating. *Appl. Surf. Sci.* **2015**, *349*, 108–115. [[CrossRef](#)]
42. Sandberg, J.; Odnevall Wallinder, I.; Leygraf, C.; Le Bozec, N. Corrosion-Induced Zinc Runoff from Construction Materials in a Marine Environment. *J. Electrochem. Soc.* **2007**, *154*, 120–131. [[CrossRef](#)]
43. Hou, D.; Zhang, K.; Hong, F.; Wu, S.; Wang, Z.; Li, M.; Wang, M. The corrosion deterioration of reinforced passivation Film: The impact of defects. *Appl. Surf. Sci.* **2022**, *582*, 152408. [[CrossRef](#)]

Disclaimer/Publisher’s Note: The statements, opinions and data contained in all publications are solely those of the individual author(s) and contributor(s) and not of MDPI and/or the editor(s). MDPI and/or the editor(s) disclaim responsibility for any injury to people or property resulting from any ideas, methods, instructions or products referred to in the content.